

# Occ3D: A Large-Scale 3D Occupancy Prediction Benchmark for Autonomous Driving

Xiaoyu Tian<sup>1\*</sup> Tao Jiang<sup>1\*</sup> Longfei Yun<sup>1\*</sup> Yue Wang<sup>2</sup> Yilun Wang<sup>1</sup> Hang Zhao<sup>1†</sup>

<sup>1</sup>IIS, Tsinghua University <sup>2</sup>NVIDIA

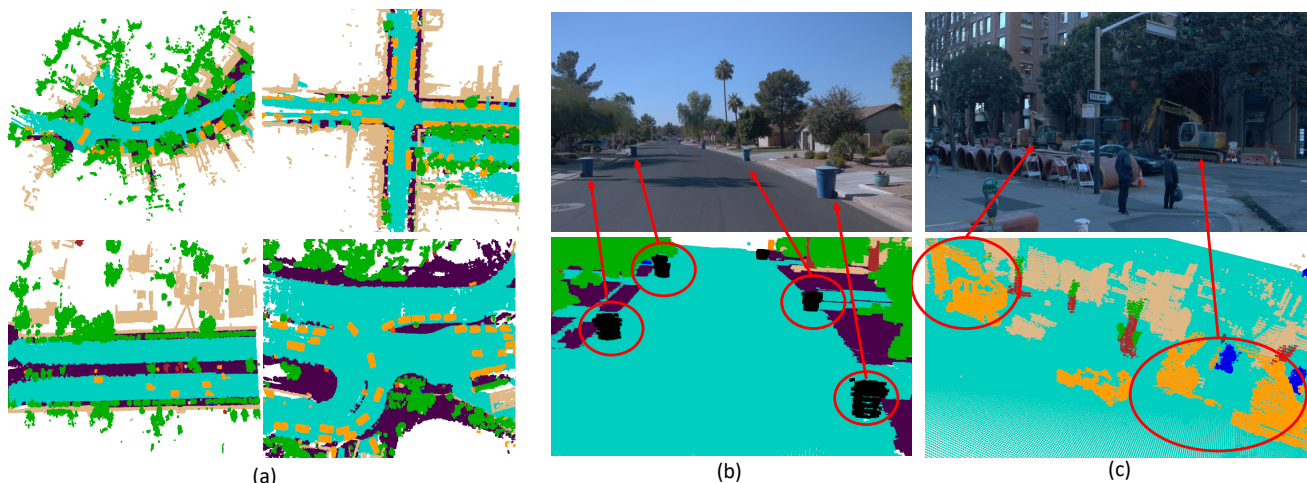


Figure 1: **The Occ3D dataset demonstrates rich semantic and geometric expressiveness.** (a) Diversity and richness of different scenes in the Occ3D dataset; (b) Out-of-vocabulary objects, also known as General Objects (GOs), that cannot be extensively enumerated in the real world; (c) Irregularly-shaped objects that 3D bounding boxes fail to provide accurate geometry.

## Abstract

Robotic perception requires the modeling of both 3D geometry and semantics. Existing methods typically focus on estimating 3D bounding boxes, neglecting finer geometric details and struggling to handle general, out-of-vocabulary objects. To overcome these limitations, we introduce a novel task for 3D occupancy prediction, which aims to estimate the detailed occupancy and semantics of objects from multi-view images. To facilitate this task, we develop a label generation pipeline that produces dense, visibility-aware labels for a given scene. This pipeline includes point cloud aggregation, point labeling, and occlusion handling. We construct two benchmarks based on the Waymo Open Dataset and the nuScenes Dataset, resulting in the Occ3D-Waymo and Occ3D-nuScenes benchmarks. Lastly, we propose a model, dubbed *Coarse-to-Fine Occupancy (CTF-Occ) net*,

which demonstrates superior performance in the 3D occupancy prediction task. This approach addresses the need for finer geometric understanding in a coarse-to-fine fashion. The code, data, and benchmarks are released at <https://tsinghua-mars-lab.github.io/Occ3D/>.

## 1. Introduction

3D perception is a crucial component in vision-based robotic systems like autonomous driving. One of the most popular visual perception tasks is 3D object detection, which estimates the locations and dimensions of objects defined in a fixed ontology tree, from monocular or stereo camera images [37, 18]. While the outputs are concise 3D bounding boxes that can be used by downstream tasks, their expressiveness is still limited as shown in Figure 1: (1) 3D bounding box representation erases the geometric details of objects, e.g. a bendy bus has two or more sections connected by rotat-

\*Equal contribution.

†Corresponding author. hangzhao@mail.tsinghua.edu.cn

ing joints, a construction vehicle has a mechanical arm that protrudes from the main body; (2) rarely seen objects, like trash or tree branch on the streets, are often ignored and not labeled in the datasets [4, 34] since object categories cannot be extensively enumerated in the ontology tree.

These limitations call for a general and coherent perception representation that can model the detailed geometry and semantics of objects both in the ontology tree and out of the ontology tree. We argue that understanding the occupancy state of each voxel in the 3D space is important to achieving this goal. A classical task in mobile robots that estimates occupancy states is Occupancy Grid Mapping (OGM) [24, 35]. OGM aggregates range measurements (like LiDAR scans) over time and estimates the probability of each voxel being occupied within a Bayesian framework. However, this solution assumes *static environments* and does not apply to *visual inputs*.

In this work, we define a comprehensive 3D scene understanding task for vision-based robotic perception, dubbed 3D Occupancy Prediction. 3D occupancy prediction jointly estimates the *occupancy state* and *semantic label* of every voxel in the scene from multi-view images. The occupancy state of each voxel can be *free*, *occupied*, or *unobserved*. Having an *unobserved* label for voxels is crucial in 3D occupancy prediction to account for visibility and exclude unobserved voxels. Semantic labels are estimated for occupied voxels. For objects with predefined categories in the dataset, their semantic labels correspond to their respective categories. Conversely, objects that are not categorized are labeled as *General Objects (GOs)*. Although GOs are seldom encountered, they are essential for robotic perception tasks with safety considerations since they are typically undetected by 3D object detection with predefined categories.

In addition, we create a label generation pipeline for the 3D occupancy prediction task to produce a dense and visibility-aware ground truth of the scene. The pipeline consists of several steps, such as temporal point cloud aggregation, dynamic object transformation, LiDAR visibility estimation, and camera visibility estimation. By leveraging ego poses and object tracks, point cloud aggregation and dynamic object transformation enhance the static scene’s density and recover the detailed geometry of dynamic objects. Furthermore, we utilize ray-casting-based methods to estimate both LiDAR and camera visibility, as visibility masks are crucial for evaluating the 3D occupancy prediction task. Building upon the public Waymo Open Dataset [34] and nuScenes Dataset [4], we produce two benchmarks for our task accordingly, Occ3D-Waymo and Occ3D-nuScenes. A series of voxel-centric semantic segmentation evaluation metrics are adopted for this task. Finally, we develop a transformer-based **Coarse-To-Fine 3D Occupancy** prediction model, named CTF-Occ. CTF-Occ aggregates 2D image features into 3D space via a cross-attention operation in an

efficient coarse-to-fine fashion.

In summary, the contributions of this paper are as follows:

1. We propose 3D Occupancy Prediction, a general and comprehensive 3D perception task for vision-based robotic applications. Occupancy prediction can represent both the semantics and geometry of any scene effectively.
2. We develop a rigorous label generation pipeline for occupancy prediction, construct two challenging datasets (Occ3D-Waymo and Occ3D-nuScenes) and establish a benchmark together with evaluation metrics to facilitate future research.
3. We propose a novel CTF-Occ network that achieves outstanding occupancy prediction performance. CTF-Occ outperforms baselines by 3.1 mIoU on Occ3D-Waymo for this challenging task.

## 2. Related Work

**3D Detection.** The goal of 3D object detection is to estimate the locations and dimensions of objects within a predefined ontology. 3D object detection is often performed in LiDAR point clouds [42, 17, 39, 40, 38, 26, 27, 9, 29]. More recently, vision-based 3D object detection has gained more attention due to its low cost and rich semantic content [32, 36, 37, 18, 21]. Several LiDAR-camera fusion methods are also proposed [25, 7, 22].

**3D Occupancy Prediction.** A related task of 3D occupancy prediction is Occupancy Grid Mapping (OGM) [24, 35], a classical task in mobile robots that aims to generate probabilistic maps from sequential noisy range measurements. Often the robot pose is known, and this mapping problem can be solved within a Bayesian framework. Some recent works further combine semantic segmentation with OGM for downstream tasks [16, 33, 28]. Note that OGM requires measurements from range sensors like LiDARs and RADARs, and also makes the assumption that the scene is static over time. Our proposed 3D occupancy prediction task does not have these constraints and can be applied in vision-only robotic systems in dynamic scenes. A concurrent work TPVFormer [15] proposes a tri-perspective view method to predict 3D occupancy. However, its output is sparse due to LiDAR supervision.

**Semantic Scene Completion.** Another related task is Semantic Scene Completion (SSC) [1, 6, 8, 2, 20], whose goal is to estimate a dense semantic space from partial observations. SSC differs from 3D occupancy prediction in two ways: (1) SSC focuses on inferring occluded regions given visible parts, while occupancy prediction does not intend

Dataset	Type	Outdoor	# Classes	Input	Ground truth	# Sequences	# Frames
NYUv2 [31]	Real-world		11	RGB-D	Mesh/Voxel	1449	795/654
NYUCAD [11]	Synthetic		11	RGB-D	Mesh/Voxel	1449	795/654
SUNCG [12]	Synthetic		11	Depth	Mesh/Voxel	45622	139368/470
SemanticKITTI [3]	Real-world	✓	28	Points/RGB	Points/Voxel	22	23201/20351
KITTI-360 [19]	Real-world	✓	19	Points	Points	11	90960
nuScenes Object Detection [4]	Real-world	✓	23	Points	Bounding Box	850	34,000
nuScenes Semantic Segmentation [4]	Real-world	✓	32	Points	Points	850	34,000
Waymo Object Detection [34]	Real-world	✓	4	Points	Bounding Box	1000	200,000
Waymo Semantic Segmentation [34]	Real-world	✓	23	Points	Points	1000	200,000
Occ3D-nuScenes	Real-world	✓	16+GO	Camera	Voxel	850	40,000
Occ3D-Waymo	Real-world	✓	14+GO	Camera	Voxel	1000	200,000

Table 1: **Dataset comparison.** Comparing Occ3D Datasets with other datasets for 3D perception, including 3D Object Detection and Semantic Segmentation and Scene Semantic Completion.

to estimate the invisible regions; (2) SSC typically works with static scenes, whereas occupancy prediction works with dynamic ones.

### 3. 3D Occupancy Prediction

#### 3.1. Task definition

Given a sequence of sensor inputs, the goal of 3D occupancy prediction is to estimate the state of each voxel in the 3D scene. Specifically, the input of the task is a  $T$ -frame historical sequence of  $N$  surround-view camera images  $\{\mathcal{I}_{i,t} \in \mathbf{R}^{H_i \times W_i \times 3}\}$ , where  $i = 1, \dots, N$  and  $t = 1, \dots, T$ .

We also assume known sensor intrinsic parameters  $\{K_i\}$  and extrinsic parameters  $\{[R_i|t_i]\}$  in each frame.

The expected outputs of the task are the states of each voxel, including `occupancy` (“occupied”, “free”) and `semantics` (category, or “unknown”). For example, a voxel on a vehicle is labeled as (“occupied”, “vehicle”), and a voxel in the free space is labeled as (“free”, None). Note that the 3D occupancy prediction framework also supports extra attributes as outputs, such as `instance IDs` and `motion vectors`; we leave them as future work.

#### 3.2. Handling general objects

One of the key advantages of the 3D semantic occupancy prediction task is the potential to handle GOs, or unknown objects. Different from 3D object detection which pre-defines categories of all the objects, 3D occupancy prediction handles arbitrary objects with occupancy grids and semantics. The geometries of objects are generally represented by voxels including out-of-vocabulary objects labeled as (“occupied”, “unknown”). This ability to represent and detect general objects makes the task more general and suitable for autonomous driving perception.

#### 3.3. Evaluation Metrics

**Mean Intersection over Union (mIoU).** Since the 3D voxel-level occupancy prediction task shares similarity with the 2D pixel-level semantic segmentation task [41], we use mean Intersection over Union (mIoU) to evaluate the performance of a model:

$$\text{mIoU} = \frac{1}{C} \sum_{c=1}^C \frac{\text{TP}_c}{\text{TP}_c + \text{FP}_c + \text{FN}_c}, \quad (1)$$

where  $\text{TP}_c$ ,  $\text{FP}_c$ , and  $\text{FN}_c$  denote the true positives, false positives and false negatives predictions for class  $c$ , respectively. Since we emphasize a vision-centric task, in practice many ground-truth voxels are not visible from images. Therefore, we only compute mIoU on regions that are visible in images.

### 4. The Occ3D Dataset

#### 4.1. Dataset Construction Pipeline

Acquiring dense voxel-level annotations for a 3D scene can be challenging and impractical. To address this, we propose a semi-automatic label generation pipeline that utilizes existing labeled 3D perception datasets. First, we sequentially aggregate points from multiple frames. Then, we voxelize the densified point clouds. And finally, we identify voxel types based on their visibility.

**Data preparation.** Our label generation pipeline requires a 3D dataset where each scene contains the following sensor data: i) a (multi-view) camera image sequence; ii) a 3D LiDAR point cloud sequence; iii) a 3D pose sequence from IMU. The intrinsic and extrinsic parameters of all the cameras and LiDARs are also required for coordinate transformation and projection. Additionally, we require human-annotated box-level semantic labels of common objects, and optionally point-level semantic labels.



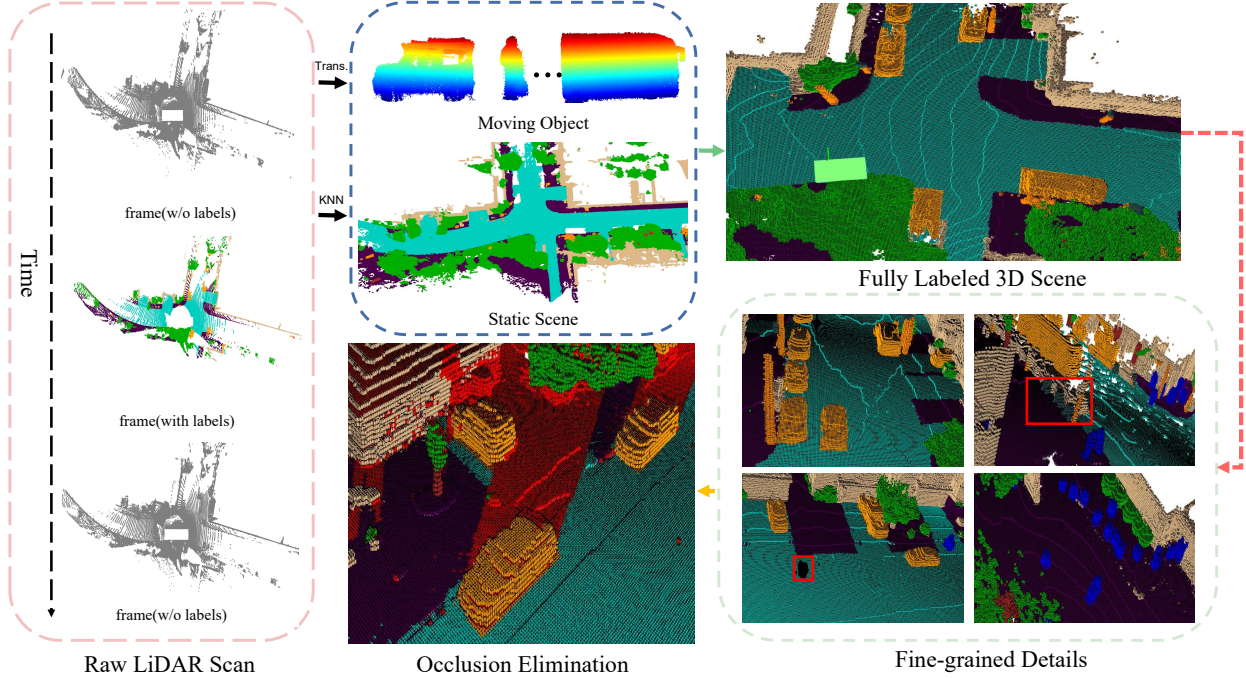


Figure 2: **The label generation pipeline.** We aggregate points of the static scenes and moving objects, respectively. Then, we transform them into a unified ego frame according to the sensor parameters. Finally, we perform occlusion reasoning to produce visibility masks for the camera views.

**Point cloud aggregation.** 3D reconstruction from sparse LiDAR observations is a classical problem in simultaneous localization and mapping (SLAM) [10]. Given a sequence of LiDAR point clouds and the IMU pose measurements at each frame, we can jointly optimize the ego-poses and aggregate the point clouds into a unified world coordinate system. However, dynamic objects suffer from motion blur after temporal aggregation. Therefore, we process dynamic objects and static objects separately. Points of dynamic objects are transformed and aggregated according to bounding box annotations at each frame and ego poses between different frames. For points of static objects, we simply aggregate them based on ego poses.

Since labeling each frame of a sequence is time-consuming, some existing datasets are labeled only at keyframes, *e.g.* nuScenes is captured at 10 Hz, but annotated at 2 Hz. Therefore, we interpolate the annotated object box sequence across time to auto-label the unannotated frames before performing the above dynamic point aggregation. Regarding the points in the unannotated frames that are not enclosed by bounding boxes, they are most likely static background stuff. Therefore we use K-Nearest Neighbor to perform major voting to determine their semantic labels. In this way, we obtain densely labeled foreground dynamic object instances and background static point clouds.

**LiDAR visibility.** To obtain a dense and regular 3D occupancy grid from aggregated LiDAR point cloud, a straightforward way is to set the voxels containing points to be “occupied” and the rest to “free”. However, since LiDAR points are sparse, some occupied voxels are not scanned by LiDAR beams, and can be mislabeled as “free”. To avoid this issue, we perform a ray casting operation to determine the visibility of each voxel. Concretely, we connect each LiDAR point with the sensor origin to form a ray, a voxel is visible if it reflects LiDAR points (“occupied”) or is traversed through by a ray (“free”); otherwise, it is tagged as “unobserved”. In this way, we produce a voxel-level LiDAR visibility mask.

**Occlusion reasoning and camera visibility.** Since we focus on a vision-centric task, we further propose an occlusion reasoning algorithm and generate a camera visibility mask, indicating whether each voxel is observed in the present multi-camera views. Concretely, for each camera view, we connect each occupied voxel center with the camera center and form a ray. Along each ray, we set the voxels before and including the first occupied voxel as “observed”, and the rest “unobserved”. Voxels not scanned by any camera rays are marked as “unobserved” as well. As shown in Figure 3, the white voxels are observed in the accumulative LiDAR view

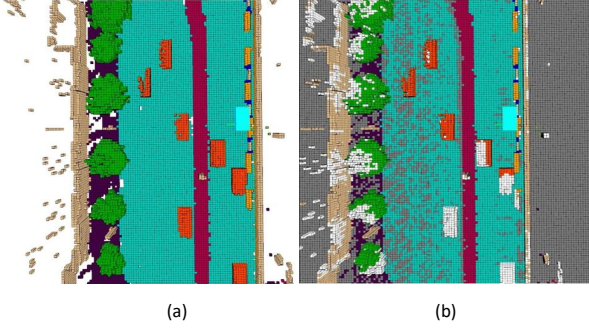


Figure 3: **Occlusion reasoning and camera visibility.** Semantic labels (left), and the camera view (right). Grey voxels are unobserved in the LiDAR view and white voxels are observed in the accumulative LiDAR view but unobserved in the current camera view.

but unobserved in the current camera view.

Note that the LiDAR visibility mask and camera visibility mask may differ due to two reasons: (1) LiDAR and cameras have different installation positions; (2) LiDAR visibility is consistent across the whole sequence, while the camera visibility differs at each timestamp.

Determining the visibility of a voxel is important for the evaluation of the 3D occupancy prediction task: evaluation is only performed on the “observed” voxels in both the LiDAR and camera views.

## 4.2. Dataset statistics

Based on the aforementioned semi-automatic annotation pipeline, we generate two 3D occupancy prediction datasets, Occ3D-Waymo and Occ3D-nuScenes. Occ3D-Waymo contains 798 sequences for training, 202 sequences for validation. It has 14 known object classes with an additional GO class. Occ3D-nuScenes contains 600 scenes for training and 150 scenes for validation. It has 16 classes with GO. Table 1 compares our proposed Occ3D dataset with existing datasets in various aspects.

## 5. Coarse-to-Fine Occupancy model

To deal with the challenging 3D occupancy prediction problem, we present a new transformer-based model named **Coarse-to-Fine Occupancy** (CTF-Occ) network. We detail the model design in this section.

### 5.1. Overall Architecture

An overview of CTF-Occ network is shown in Figure 4. First, 2D image features are extracted from multi-view images with an image backbone. Then, 3D voxel queries aggregate 2D image features into 3D space via a cross-attention operation. Our approach involves using a pyramid voxel

encoder that progressively improves voxel feature representations through incremental token selection and spatial cross-attention in a coarse-to-fine fashion. This method enhances the spatial resolution and refines the detailed geometry of objects, ultimately leading to more accurate 3D occupancy predictions. Additionally, we utilize an implicit occupancy decoder, which allows for arbitrary resolution output.

### 5.2. Coarse-to-Fine Voxel Encoder

The 3D occupancy prediction task involves modeling more intricate geometric structures of objects compared to 3D object detection. To account for this, our approach preserves the 3D voxel space without compressing the height. Initially, we adopt a learnable voxel embedding with a shape of  $H \times W \times L$  to aggregate multi-view image features into 3D grid space. We then stack multiple CTF voxel encoders to enable multi-scale interactions. Each voxel encoder at every pyramid level consists of three components: an incremental token selection module, a voxel spatial cross-attention module, and a convolutional feature extractor.

**Incremental Token Selection.** As mentioned before, the task of predicting 3D occupancy requires a detailed representation of geometry, but this can result in significantly computational and memory costs if all 3D voxel tokens are used to interact with regions of interest in the multi-view images. Given that most 3D voxel grids in a scene are empty, we propose an incremental token selection strategy that selectively chooses foreground and uncertain voxel tokens in cross-attention computation. This strategy enables adaptive and efficient computation without sacrificing accuracy. Specifically, at the beginning of each pyramid level, each voxel token is fed into a binary classifier to predict whether this voxel is empty or not. We use the binary ground-truth occupancy map as supervision to train the classifier. In our approach, we select the K-most uncertain voxel tokens for the subsequent feature refinement. There are three ways to define the K-most uncertain voxels: those with probabilities near 0.5, K non-empty voxels with the highest scores, or a combination of both types of voxels with a specific percentage. Our ablation study demonstrates that choosing foreground voxels at an early stage is a more desirable alternative.

**Spatial Cross Attention.** At every level of the pyramid, we first select the top-K voxel tokens and then aggregate the corresponding image features. In particular, we apply spatial cross-attention to further refine the voxel features. The 3D spatial cross-attention is defined by:

$$\text{SCA}(V_p, F_t) = \sum_{j=1}^{N_{\text{ref}}} \text{DFA}(V_p, \mathcal{P}(p, i, j), F_t^i), \quad (2)$$

where  $i, j$  are the indices of the camera view and reference points. For each selected voxel token query  $V_p$ , a projection

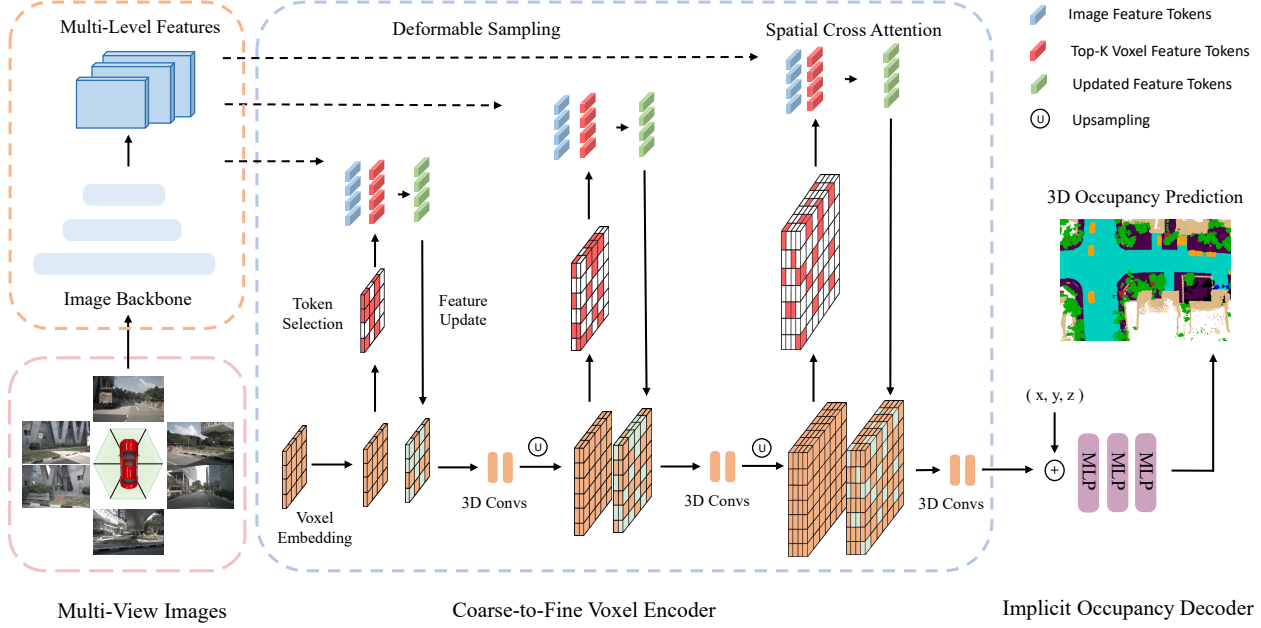


Figure 4: **The model architecture of CTF-Occ network.** Our CTF-Occ network mainly consists of three parts: the image backbone, the coarse-to-fine voxel encoder, and the implicit occupancy decoder.

$\mathcal{P}(p, i, j)$  is implemented to attain the  $j$ -th reference point on the  $i$ -th image.  $F_t^i$  denotes the features of the  $i$ -th camera view. We calculate the real-world location  $(x', y', z')$  of the reference points corresponding to the query  $V_p$  located at  $p = (x, y, z)$  as:

$$\begin{aligned} x' &= \left(x - \frac{W}{2}\right) \times s \\ y' &= \left(y - \frac{H}{2}\right) \times s \\ z' &= \left(z - \frac{L}{2}\right) \times s \end{aligned} \quad (3)$$

where  $H, W, L$  are the 3D grid spatial shapes at the current pyramid level and  $s$  is the size of the voxel grids.

**Convolutional Feature Extractor.** Once we apply deformable cross-attention to the relevant image features, we proceed to update the features of the foreground voxel tokens. Then, we use a series of stacked convolutions to enhance feature interaction throughout the entire 3D voxel feature maps. At the end of the current level, we upsample the 3D voxel features using trilinear interpolation. The overall process can be described as

$$F_{S_{i+1}} = \text{Up}(\text{Convs}(F_{S_i})), \quad (4)$$

where  $F_{S_i} \in \mathbb{R}^{W_i \times H_i \times L_i \times C}$ ,  $F_{S_{i+1}} \in \mathbb{R}^{W_{i+1} \times H_{i+1} \times L_{i+1} \times C}$  and  $W_{i+1} = 2W_i$ ,  $H_{i+1} = 2H_i$ ,  $L_{i+1} = 2L_i$ .

### 5.3. Implicit Occupancy Decoder

The CTF voxel encoder generates voxelized feature output  $V_{out} \in \mathbb{R}^{W \times H \times L \times C}$ . Then the voxel features  $V_{out}$  are fed into several MLPs to obtain the final occupancy prediction  $O \in \mathbb{R}^{W \times H \times L \times C'}$ , where  $C'$  is the number of the semantic classes. Furthermore, we introduce an implicit occupancy decoder that can offer arbitrary resolution output by utilizing implicit neural representations. The implicit decoder is implemented as an MLP that outputs a semantic label by taking two inputs: a voxel feature vector extracted by the voxel encoder and a 3D coordinate inside the voxel. The process can be described as

$$O_{(x,y,z)} = \text{MLP}(\text{Concat}(F_{V_{(x',y',z')}}), (x, y, z)). \quad (5)$$

### 5.4. Loss Function

To optimize the occupancy prediction, we use the OHEM [30] loss for model training  $\mathcal{L}_{occ} = \sum_k W_k \mathcal{L}(g_k, p_k)$ , where  $W_k$ ,  $g_k$ , and  $p_k$  represent the loss weight, the label, and the prediction result for the  $k$ -th semantic class. In addition, we supervise the binary classification head in each pyramid level with binary voxel masks. The binary voxel masks are generated by processing the semantic occupancy label at each spatial resolution  $s_i$  using  $f(g, s_i)$ , and the output of the binary classification head in the  $i$ -th level is denoted as  $p_i$ . The loss for the binary classification is defined as  $\mathcal{L}_{bin} = \sum_i \mathcal{L}(f(g, s_i), p_i)$ , where  $i$  represents the  $i$ -th pyramid level. Finally, the overall loss is  $\mathcal{L} = \mathcal{L}_{occ} + \mathcal{L}_{bin}$ .



Method	Input	others	barrier	bicycle	bus	car	construction vehicle	motorcycle	pedestrian	traffic cone	trailer	truck	driveable surface	other flat	sidewalk	terrain	manmade	vegetation	mIoU
MonoScene [5]	C	1.75	7.23	4.26	4.93	9.38	5.67	3.98	3.01	5.90	4.45	7.17	14.91	6.32	7.92	7.43	1.01	7.65	6.06
BEVDet [14]	C	2.09	15.29	0.0	4.18	12.97	1.35	0.0	0.43	0.13	6.59	6.66	52.72	19.04	26.45	21.78	14.51	15.26	11.73
BEVFormer [18]	C	5.85	37.83	17.87	40.44	42.43	7.36	23.88	21.81	20.98	22.38	30.70	55.35	28.36	36.0	28.06	20.04	17.69	26.88
<b>CTF-Occ (Ours)</b>	C	8.09	39.33	20.56	38.29	42.24	16.93	24.52	22.72	21.05	22.98	31.11	53.33	33.84	37.98	33.23	20.79	18.0	28.53

Table 2: 3D occupancy prediction performance on the Occ3D-nuScenes dataset. C, L denote camera and LiDAR.

OHEM Loss	Token Selection Strategy			IoU		mIoU
	random	uncertain	top-k	PED	CC	
			✓	0	0.03	10.06
✓	✓			5.07	12.95	16.62
✓		✓		6.27	13.85	17.37
✓			✓	7.04	14.16	17.63

Table 3: Ablation study on our model components, performed on the Occ3D-Waymo dataset.

## 6. Experiments

### 6.1. Experimental Setup

**Dataset.** Occ3D-Waymo contains 1,000 publicly available sequences in total, where 798 scenes for training and 202 scenes for validation. The scene range is set from -40m to 40m along X and Y axis, and from -5m to 7.8m along Z axis. Occ3D-nuScenes contains 700 training scenes and 150 validation scenes. The occupancy scope is defined as -40m to 40m for X and Y axis, and -1m to 5.4m for the Z axis. We choose a voxel size of 0.4m to conduct our experiments on both two datasets.

**Architecture.** We employ ResNet-101 [13] pretrained on FCOS3D [36] as the image backbone, and the image size is resized to (640 × 960) for Occ3D-Waymo and (928 × 1,600) for Occ3D-nuScenes. We adopt the same architecture setting of our CTF-Occ network for both two datasets except the resolution of the z-axis. The shape of the voxel embedding is (200 × 200) with 256 channels. The voxel embedding will first pass through four encoder layer without token selection. There are three pyramid stage levels for the Occ3D-Waymo dataset and the resolution of the z-axis in each stage is 8, 16, and 32. The resolution of the z-axis in each stage for the Occ3D-nuScenes dataset is 8 and 16 for two pyramid stages. Each stage contains one SCA layer and the top-k ratio for the incremental token selection strategy is set to 0.2 for all pyramid stages.

We also extend two main-stream BEV models – BEVDet[14] and BEVFormer [18] to the 3D occupancy prediction task. We replace their original detection decoders with the occupancy decoder adopted in our CTF-Occ network and remain their BEV feature encoders. Following

their original setting, we adopt ResNet101-DCN that initialized from FCOS3D [36] checkpoint as the image backbone.

**Implementation Details.** We use AdamW optimizer [23] and cosine learning rate scheduler with a learning rate set to 2e-4. Unless otherwise specified, all models are trained for 24 epochs for comparison and 8 epochs for the ablation study.

### 6.2. Comparing with previous methods

**Occ3D-nuScenes.** Table 2 shows the performance of 3D occupancy prediction compared to related methods on the Occ3D-nuScenes dataset. It can be observed that our method performs better in all classes than previous baseline methods under the IoU metric. The observations are consistent with those in the Occ3D-Waymo dataset.

**Occ3D-Waymo.** We compare the performance of our CTF-Occ network with state-of-the-art models on our newly proposed Occ3D-Waymo dataset. Results are shown in Table 4. Our method outperforms previous methods by remarkable margins, *i.e.* increasing the mIoU by 3.11. Especially for some small objects such as pedestrians and bicycles, our method surpasses the baseline method by 4.11 and 13.0 IoU respectively. This is because we capture the features in the 3D voxel space without compressing the height, which will preserve the detailed geometry of objects. The results indicate the effectiveness of our coarse-to-fine voxel encoder.

### 6.3. Ablation study

In this section, we ablate the choices of incremental token selection and OHEM loss. Table 3 shows the results. CC represents traffic cones and PED represents pedestrians. We focus on CC and PED to verify the effectiveness of our

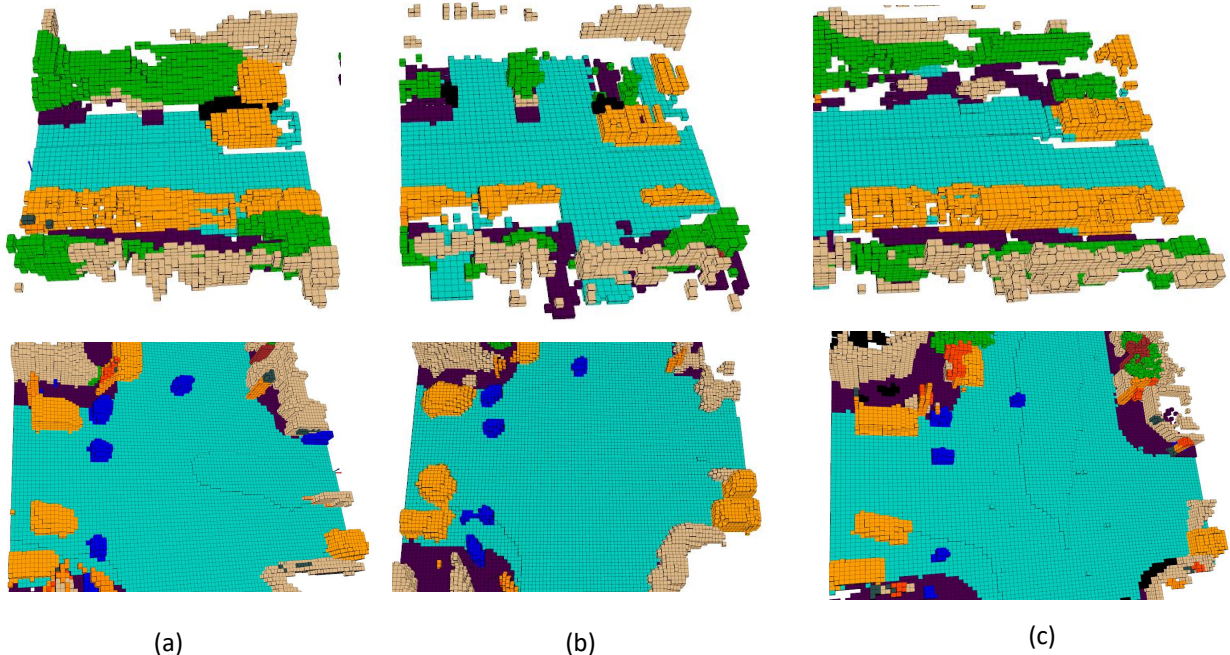


Figure 5: **Qualitative results.** Comparing (a) our CTF-Occ network, (b) BEVFormer-Occ, and (c) the ground truth labels on the Occ3D-Waymo dataset.

Method	Input	general object	vehicle	bicyclist	pedestrian	sign	traffic light	car	construction cone	bicycle	motorcycle	building	vegetation	tree trunk	road	sidewalk	mIoU
BEVDet [14]	C	0.13	13.06	2.17	10.15	7.80	5.85	4.62	0.94	1.49	0.0	7.27	10.06	2.35	48.15	34.12	9.88
BEVFormer [18]	C	2.59	25.76	13.87	4.11	14.23	3.35	8.41	7.54	3.45	0.0	18.46	16.21	6.87	67.72	41.68	15.62
<b>CTF-Occ (Ours)</b>	C	6.26	28.09	14.66	8.22	15.44	10.53	11.78	13.62	16.45	0.65	18.63	17.3	8.29	67.99	42.98	18.73

Table 4: 3D occupancy prediction performance on the Occ3D-Waymo dataset. C, L denote camera and LiDAR.

implementation on small objects. Both techniques improve performance. Using OHEM loss and top-k token selection produces the best performance. Without the OHEM loss, we only get 10.06 mIoU. Combining the OHEM loss with a random token selection strategy achieves 14.75 mIoU. Using an uncertain token selection strategy with OHEM loss achieve 17.37 mIoU. For token selection, uncertain selection and top-k selection are on par and they significantly outperform the random selection as expected.

#### 6.4. Qualitative results

We compare our CTF-Occ network outputs with the state-of-the-art method BEVFormer-Occ on the Occ3D-Waymo dataset in Fig 5. We can see that our CTF-Occ network outputs a more detailed voxel geometry than the BEVFormer-Occ results. In addition, our voxel decoder is capable of producing outputs at any resolution, without being constrained

by the resolution of the ground truth data.

## 7. Conclusion

We present Occ3D, a large-scale 3D occupancy prediction benchmark for visual perception. This benchmark includes a data generation protocol, two datasets, and a model CTF-Occ network for this task. They will all be open-sourced to facilitate future research. Our study has revealed that semantic occupancy offers a more expressive and enriched representation of objects. In addition, it provides a unified representation of known and unknown objects, which is crucial for robotics perception in the wild. Apart from its direct usage, this benchmark opens up several avenues for future research. For example, adding instance IDs to semantic voxels will essentially change the task to panoptic segmentation and provide even richer information.



## References

- [1] Iro Armeni, Sasha Sax, Amir R Zamir, and Silvio Savarese. Joint 2d-3d-semantic data for indoor scene understanding. *arXiv preprint arXiv:1702.01105*, 2017. 2
- [2] Jens Behley, Martin Garbade, Andres Milioto, Jan Quenzel, Sven Behnke, Cyrill Stachniss, and Juergen Gall. A dataset for semantic segmentation of point cloud sequences. *arXiv preprint arXiv:1904.01416*, 2(3), 2019. 2
- [3] J. Behley, M. Garbade, A. Milioto, J. Quenzel, S. Behnke, C. Stachniss, and J. Gall. SemanticKITTI: A Dataset for Semantic Scene Understanding of LiDAR Sequences. In *Proc. of the IEEE/CVF International Conf. on Computer Vision (ICCV)*, 2019. 3
- [4] Holger Caesar, Varun Bankiti, Alex H Lang, Sourabh Vora, Venice Erin Liong, Qiang Xu, Anush Krishnan, Yu Pan, Giancarlo Baldan, and Oscar Beijbom. nuscenes: A multi-modal dataset for autonomous driving. In *Proceedings of the IEEE/CVF conference on computer vision and pattern recognition*, pages 11621–11631, 2020. 2, 3
- [5] Anh-Quan Cao and Raoul de Charette. Monoscene: Monocular 3d semantic scene completion. In *Proceedings of the IEEE/CVF Conference on Computer Vision and Pattern Recognition*, pages 3991–4001, 2022. 7
- [6] Angel Chang, Angela Dai, Thomas Funkhouser, Maciej Halber, Matthias Niessner, Manolis Savva, Shuran Song, Andy Zeng, and Yinda Zhang. Matterport3d: Learning from rgb-d data in indoor environments. *arXiv preprint arXiv:1709.06158*, 2017. 2
- [7] Xuanyao Chen, Tianyuan Zhang, Yue Wang, Yilun Wang, and Hang Zhao. Futr3d: A unified sensor fusion framework for 3d detection. *arXiv preprint arXiv:2203.10642*, 2022. 2
- [8] Angela Dai, Angel X Chang, Manolis Savva, Maciej Halber, Thomas Funkhouser, and Matthias Nießner. Scannet: Richly-annotated 3d reconstructions of indoor scenes. In *Proceedings of the IEEE conference on computer vision and pattern recognition*, pages 5828–5839, 2017. 2
- [9] Zhipeng Ding, Xu Han, and Marc Niethammer. Votenet: A deep learning label fusion method for multi-atlas segmentation. In *International Conference on Medical Image Computing and Computer-Assisted Intervention*, pages 202–210. Springer, 2019. 2
- [10] Hugh Durrant-Whyte and Tim Bailey. Simultaneous localization and mapping: part i. *IEEE robotics & automation magazine*, 13(2):99–110, 2006. 4
- [11] Michael Firman, Oisín Mac Aodha, Simon Julier, and Gabriel J Brostow. Structured prediction of unobserved voxels from a single depth image. In *Proceedings of the IEEE Conference on Computer Vision and Pattern Recognition*, pages 5431–5440, 2016. 3
- [12] Saurabh Gupta, Ross Girshick, Pablo Arbeláez, and Jitendra Malik. Learning rich features from rgb-d images for object detection and segmentation. In *Computer Vision—ECCV 2014: 13th European Conference, Zurich, Switzerland, September 6–12, 2014, Proceedings, Part VII 13*, pages 345–360. Springer, 2014. 3
- [13] Kaiming He, Xiangyu Zhang, Shaoqing Ren, and Jian Sun. Deep residual learning for image recognition. In *Proceedings of the IEEE conference on computer vision and pattern recognition*, pages 770–778, 2016. 7
- [14] Junjie Huang, Guan Huang, Zheng Zhu, and Dalong Du. Bevdet: High-performance multi-camera 3d object detection in bird-eye-view. *arXiv preprint arXiv:2112.11790*, 2021. 7, 8
- [15] Yuanhui Huang, Wenzhao Zheng, Yunpeng Zhang, Jie Zhou, and Jiwen Lu. Tri-perspective view for vision-based 3d semantic occupancy prediction. *arXiv preprint arXiv:2302.07817*, 2023. 2
- [16] Hyeon-Seok Jeon, Dong-Suk Kum, and Woo-Yeol Jeong. Traffic scene prediction via deep learning: Introduction of multi-channel occupancy grid map as a scene representation. In *2018 IEEE Intelligent Vehicles Symposium (IV)*, pages 1496–1501. IEEE, 2018. 2
- [17] Alex H Lang, Sourabh Vora, Holger Caesar, Lubing Zhou, Jiong Yang, and Oscar Beijbom. PointPillars: Fast Encoders for Object Detection from Point Clouds. In *CVPR*, pages 12697–12705, 2019. 2
- [18] Zhiqi Li, Wenhao Wang, Hongyang Li, Enze Xie, Chonghao Sima, Tong Lu, Qiao Yu, and Jifeng Dai. Bevformer: Learning bird’s-eye-view representation from multi-camera images via spatiotemporal transformers. *arXiv preprint arXiv:2203.17270*, 2022. 1, 2, 7, 8
- [19] Yiyi Liao, Jun Xie, and Andreas Geiger. KITTI-360: A novel dataset and benchmarks for urban scene understanding in 2d and 3d. *arXiv preprint arXiv:2109.13410*, 2021. 3
- [20] Yiyi Liao, Jun Xie, and Andreas Geiger. Kitti-360: A novel dataset and benchmarks for urban scene understanding in 2d and 3d. *IEEE Transactions on Pattern Analysis and Machine Intelligence*, 2022. 2
- [21] Yingfei Liu, Tiancai Wang, Xiangyu Zhang, and Jian Sun. Petr: Position embedding transformation for multi-view 3d object detection. *arXiv preprint arXiv:2203.05625*, 2022. 2
- [22] Zhijian Liu, Haotian Tang, Alexander Amini, Xinyu Yang, Huizi Mao, Daniela Rus, and Song Han. Bevfusion: Multi-task multi-sensor fusion with unified bird’s-eye view representation. *arXiv preprint arXiv:2205.13542*, 2022. 2
- [23] Ilya Loshchilov and Frank Hutter. Decoupled weight decay regularization. *arXiv preprint arXiv:1711.05101*, 2017. 7
- [24] Hans Moravec and Alberto Elfes. High resolution maps from wide angle sonar. In *Proceedings. 1985 IEEE international conference on robotics and automation*, volume 2, pages 116–121. IEEE, 1985. 2
- [25] Charles R Qi, Wei Liu, Chenxia Wu, Hao Su, and Leonidas J Guibas. Frustum PointNets for 3D Object Detection from RGB-D Data. In *CVPR*, pages 918–927, 2018. 2
- [26] Charles R Qi, Hao Su, Kaichun Mo, and Leonidas J Guibas. PointNet: Deep Learning on Point Sets for 3D Classification and Segmentation. In *CVPR*, pages 652–660, 2017. 2
- [27] Charles Ruizhongtai Qi, Li Yi, Hao Su, and Leonidas J Guibas. PointNet++: Deep Hierarchical Feature Learning on Point Sets in a Metric Space. In *NeurIPS*, pages 5099–5108, 2017. 2
- [28] Thomas Roddick and Roberto Cipolla. Predicting semantic map representations from images using pyramid occupancy networks. In *Proceedings of the IEEE/CVF Conference*

- on *Computer Vision and Pattern Recognition*, pages 11138–11147, 2020. 2
- [29] Danila Rukhovich, Anna Vorontsova, and Anton Konushin. Fcaf3d: fully convolutional anchor-free 3d object detection. In *Computer Vision–ECCV 2022: 17th European Conference, Tel Aviv, Israel, October 23–27, 2022, Proceedings, Part X*, pages 477–493. Springer, 2022. 2
  - [30] Abhinav Shrivastava, Abhinav Gupta, and Ross Girshick. Training region-based object detectors with online hard example mining. In *Proceedings of the IEEE conference on computer vision and pattern recognition*, pages 761–769, 2016. 6
  - [31] Nathan Silberman, Derek Hoiem, Pushmeet Kohli, and Rob Fergus. Indoor segmentation and support inference from rgb-d images. *ECCV (5)*, 7576:746–760, 2012. 3
  - [32] Andrea Simonelli, Samuel Rota Buló, Lorenzo Porzi, Manuel López-Antequera, and Peter Kotschieder. Disentangling monocular 3d object detection. In *Proceedings of the IEEE/CVF International Conference on Computer Vision*, pages 1991–1999, 2019. 2
  - [33] Liat Sless, Bat El Shlomo, Gilad Cohen, and Shaul Oron. Road scene understanding by occupancy grid learning from sparse radar clusters using semantic segmentation. In *Proceedings of the IEEE/CVF International Conference on Computer Vision Workshops*, pages 0–0, 2019. 2
  - [34] Pei Sun, Henrik Kretschmar, Xerxes Dotiwalla, Aurelien Chouard, Vijaysai Patnaik, Paul Tsui, James Guo, Yin Zhou, Yuning Chai, Benjamin Caine, et al. Scalability in perception for autonomous driving: Waymo open dataset. In *Proceedings of the IEEE/CVF conference on computer vision and pattern recognition*, pages 2446–2454, 2020. 2, 3
  - [35] Sebastian Thrun. Probabilistic robotics. *Communications of the ACM*, 45(3):52–57, 2002. 2
  - [36] Tai Wang, Xinge Zhu, Jiangmiao Pang, and Dahua Lin. Fcos3d: Fully convolutional one-stage monocular 3d object detection. *arXiv preprint arXiv:2104.10956*, 2021. 2, 7
  - [37] Yue Wang, Vitor Campagnolo Guizilini, Tianyuan Zhang, Yilun Wang, Hang Zhao, and Justin Solomon. Detr3d: 3d object detection from multi-view images via 3d-to-2d queries. In *Conference on Robot Learning*, pages 180–191. PMLR, 2022. 1, 2
  - [38] Yue Wang and Justin M. Solomon. Object dgcn: 3d object detection using dynamic graphs. In *2021 Conference on Neural Information Processing Systems (NeurIPS)*, 2021. 2
  - [39] Yan Yan, Yuxing Mao, and Bo Li. SECOND: Sparsely Embedded Convolutional Detection. *Sensors*, 18(10):3337, 2018. 2
  - [40] Tianwei Yin, Xingyi Zhou, and Philipp Krähenbühl. Center-based 3D Object Detection and Tracking. *arXiv preprint arXiv:2006.11275*, 2020. 2
  - [41] Bolei Zhou, Hang Zhao, Xavier Puig, Sanja Fidler, Adela Barriuso, and Antonio Torralba. Scene parsing through ade20k dataset. In *Proceedings of the IEEE conference on computer vision and pattern recognition*, pages 633–641, 2017. 3
  - [42] Yin Zhou and Oncel Tuzel. VoxelNet: End-to-End Learning for Point Cloud Based 3D Object Detection. In *CVPR*, pages 4490–4499, 2018. 2